Molecular Simulation of Glassy Polystyrene: Size Effects on Gas Solubilities

Thomas R. Cuthbert and Norman J. Wagner*

Center for Molecular and Engineering Thermodynamics, Department of Chemical Engineering, University of Delaware, Newark, Delaware 19716

Michael E. Paulaitis

Department of Chemical Engineering, Johns Hopkins University, Baltimore, Maryland 21218

Received May 30, 1996; Revised Manuscript Received October 7, 1996[⊗]

ABSTRACT: Polystyrene structures, consisting of a single chain of 40, 62, 171, or 364 monomers folded into periodic cells, were generated by a new Gaussian lattice method. The different structures were simulated to study system size effects on the calculated excess chemical potentials of five gases (Ar, O_2, N_2, CH_4, and CO_2) in amorphous polystyrene glass. Excess chemical potentials were calculated using the test-particle insertion method and a modified excluded-volume map sampling algorithm. For the largest structure, we observe that the excess chemical potential decreases linearly with the depth of the Lennard-Jones well of the penetrant, in agreement with experiment. However, we find that the smaller structures are, on average, unable to form cavities of sufficient size to accommodate CH_4 and CO_2 (the larger penetrants). We also show that the instantaneous excess chemical potential distribution provides a sensitive probe of system size effects on polymer architecture.

I. Introduction

The application of atomistic simulations to study transport properties of penetrants in glassy polymers has become computationally tractable in recent years due to the availability of more powerful computers and more efficient simulation algorithms. An appealing feature of these simulations is that they offer an avenue for exploring polymer/penetrant properties that are not readily accessible from experiments. For example, penetrant transport through polymer membranes is measured in terms of membrane permeability, defined as the product of the diffusion coefficient D and the solubility S

$$P = DS \tag{1}$$

Independent determinations of D and S are possible from atomistic simulations,[1−11] such that the influence of chemical architecture and polymer morphology on the overall permeability can be examined in detail. Atomistic simulations not only provide a method for estimated both D and S but also offer insights into the molecular mechanisms of penetrant transport through the polymer. The ability to calculate changes in permeability resulting from modifications of the chemical and structural properties of polymer membranes suggests a direct application of atomistic simulations to improve membrane performance and ultimately to design new membranes from first principles.

To date, atomistic simulations have been limited in both the size of the polymer microstructures and the number of independent starting configurations that can be considered.[12−16] These limitations are a consequence of the demanding computational loads required to generate and process polymer glass structures. Typical simulations of glassy polymers at densities between 0.8 and 1.4 g/cm^3 involve 500−1000 explicit or united atoms with chains packed into a periodic simulation cell 18−30 Å on each side. These structures are validated by comparing properties such as the cohesive energy density and X-ray or neutron structure factors against experimental values.[12,15,17] Although the cohesive energy densities and structure factors obtained from simulated glass structures can be reasonably matched to experimental values,[12,15,17] the calculated diffusion coefficients and solubilities of simple gases (e.g., He, H_2, O_2, N_2, CH_4) often deviate by as much as 1−3 orders of magnitude.[2,4,5,7,9,10] Reasonable quantitative agreement for diffusion coefficients has been achieved only in a few specific cases: notably, for methane in polyethylene[6] and in poly(dimethylsiloxane)[4] as well as for helium in polycarbonate.[11] One proposed explanation for these discrepancies is that potentials optimized to yield the correct structure may not necessarily work for transport properties, as is well-known for even simple fluids.[18]

Another possible explanation for observed discrepancies in both the diffusion coefficients and solubilities is limited system sizes. It has long been known[19] that simulations of Lennard-Jones (LJ) fluids containing too few particles exhibit both unphysical structures and inaccurate dynamic properties. Restricting system size is expected to have a significant impact on penetrant transport through the polymer as well. For simple gases, diffusion in a polymer glass is believed to occur through a cavity "hopping" mechanism,[4,20,21] whereby a penetrant is localized in a cavity in the glass structure and sporadically undergoes jumps to nearby cavities. The cavities to which the penetrant may successfully jump not only must be spatially close (5−10 Å)[20] but also must be large enough to accept the penetrant. Thus, penetrant diffusivity will be sensitive to both the size distribution and the spatial distribution of the cavities. The solubility of a penetrant is likewise influenced by the cavity size distributions as seen from scaled particle theory (SPT).[22] The solubility of a penetrant in SPT is proportional to the probability of inserting a cavity of radius R into the polymer matrix such that the cavity does not overlap the van der Waals volume of any polymer atom. Consequently, any simulation artifacts that alter the distribution and/or struc-

* Corresponding author. E-mail: wagner@che.udel.edu.
[⊗] Abstract published in *Advance ACS Abstracts,* May 1, 1997.

S0024-9297(96)00776-0 CCC: $14.00

ture of available cavities would deleteriously affect both the calculated diffusivity and solubility of a penetrant.

Unlike simple fluids, the effect of system size on atomistic simulations of gas permeation in polymers has not been thoroughly studied, the principle reason being the high computational expense of generating and processing appropriate structures. In the few cases where system size effects have been examined, conflicting results for the diffusion of simple gases have been reported. Gusev *et al.*[8] found a 30% difference for helium diffusion in amorphous polycarbonate structures between simulation boxes 33 and 50 Å on a side. In contrast, Müller-Plathe *et al.*[3] found no statistical difference in the oxygen diffusion coefficient in atactic polypropylene structures with simulation box lengths of 20 and 30 Å. To our knowledge, there have been no such studies of system size effects on the solubility of simple gases in polymer glasses.

In this work we examine the influence of system size on the calculated solubility of gases in polymer glasses. Simple gases are chosen because both experimental solubility measurements[23] and atomistic simulations[2] demonstrate that the logarithm of the Henry's law constant of these penetrants in polymer glasses correlates with the Lennard-Jones well-depth parameter of the gas. As will be shown, this correlation enables a straightforward characterization of system size effects for different gases, decoupled from questions about the accuracy of potential parameters. Atactic polystyrene was chosen as our model, glassy polymer because it is well-characterized experimentally and solubility data exist for the simple gases of interest. To generate a size range of polystyrene glass structures, we apply a recently developed algorithm for efficiently generating large structures of amorphous polymers in a periodic simulation cell.[24] A new algorithm, based on excluded-volume map sampling (EVMS),[25] is presented here and implemented to efficiently calculate excess chemical potentials (and hence gas solubilities) in these polymer structures. In the following, we first present our analysis of the solubility data, followed by a presentation of our simulation method. The method is then applied to calculate solubilities of N_2, O_2, Ar, CH_2, and CO_2 in polystyrene glasses of different simulation sizes. The results are interpreted in terms of the distribution of the excess chemical potential as a function of system size. The subsequent analysis demonstrates the sensitivity of gas solubility to the availability of cavities large enough to accommodate the gas molecule.

II. Theoretical Analysis of Gas Sorption

A. Thermodynamics of Gas Sorption. The phenomenological dual-mode sorption model is widely used to describe gas sorption data in polymer glasses. We present here how the infinite-dilution chemical potential of the sorbed gas can be extracted from the experimentally determined dual-mode sorption expression. A relationship between the amount of gas sorbed in the polymer and its partial pressure in the vapor phase is given by the dual-mode sorption model as[23]

$$C_i = kP_i + \frac{C_H b P_i}{1 + bP_i} \tag{2}$$

where C_i is the molar concentration of gas in the polymer (mol/cm^3), P_i is the partial pressure of the gas, k is related to a Henry's law constant defined within the context of the dual-mode model, and C_H and b are empirical constants. In the low-pressure limit, eq 2 reduces to

$$C_i = (k + C_H b)P_i = K_H P_i \tag{3}$$

where K_H is an apparent Henry's law constant. From standard thermodynamic relations,[26] the Henry's law constant for species i is

$$H_i = \lim_{x_i \to 0} \frac{\bar{f}_i}{x_i} \tag{4}$$

with $\bar{f}_i$ the fugacity of species i and x, its mole fraction in the phase of interest. For an ideal-gas vapor phase in equilibrium with the polymer phase, eq 4 is written as

$$H_i = \lim_{x_i \to 0} \frac{P_i}{x_i} = \lim_{n_i \to 0} \frac{P_i n_p}{n_i} \tag{5}$$

Here n_p is the total number of moles and n_i is the number of moles of species i in the polymer phase. The Henry's law constant is related to the apparent Henry's law constant, K_H, by rewriting eq 5 as follows:

$$H_i = \lim_{C_i \to 0} \frac{P_i \rho_p}{C_i} = \frac{1}{K_H} \lim_{C_i \to 0} \rho_p = \frac{\rho_p^\circ}{K_H} \tag{6}$$

where ρ_p is the molar density of the polymer phase and ρ_p° is the molar density of the pure polymer. Equation 6 enables extraction of Henry's law constants from the empirically determined constants: b, C_H, and k.

The relationship between the Henry's law constant and the infinite-dilution excess chemical potential is obtained from the definition of the excess chemical potential of species i relative to an ideal gas mixture (IGM):

$$\mu_i^{ex} = -k_b T \ln \frac{\bar{f}_i}{x_i f_i} \tag{7}$$

where f_i is the pure-component fugacity of species i. If the IGM is chosen to be at the same T, x_i, and ρ of the actual mixture:[27]

$$\mu_i^{ex} = -k_b T \ln \frac{\bar{f}_i}{x_i \rho_p k_b T} \tag{8}$$

and taking the infinite-dilution limit,

$$\mu_{x_i \to 0}^{ex} = -k_b T \ln \frac{H_i}{\rho_p^\circ k_b T} \tag{9}$$

Combining eqs 6 and 9, we obtain the desired relationship between the infinite-dilution excess chemical potential and the dual-mode sorption parameters extracted from experimental gas solubilities in glassy polymers:

$$\mu_{x_i \to 0}^{ex} = -k_b T \ln \frac{1}{K_H k_b T} \tag{10}$$

This equation enables calculation of the excess chemical potentials from experimental gas sorption isotherms, which can then be compared to those calculated directly from our simulations.

B. Widom's Test Particle Insertion Method. The infinite-dilution excess chemical potential of a gas sorbed in our polystyrene structures is obtained by applying Widom's test-particle insertion method.[28] In this technique, the chemical potential of species i in an N-particle system relative to an ideal gas mixture (IGM)

is related to the potential energy of inserting a "test" particle into the system at randomly chosen positions. The expression for the excess chemical potential is

$$\beta\mu_i^{ex}(\rho,T) = -\ln \langle \exp(-\beta\Phi_t)\rangle_N \qquad (11)$$

where $\beta = 1/k_bT$, $\Phi_t = (\sum_{j=1}^{N}\phi_{tj})$ is the total potential energy of interaction between the test particle and the N particles of the system, and $\mu_i^{ex}(\rho,T)$ is the excess chemical potential of species i at temperature T and number density $\rho = N/V$. The brackets $\langle ...\rangle_N$ denote the canonical ensemble average over the original N-particle system (without the test particle) at the T and ρ of interest. Equation 11 suggests a computational algorithm for calculationg μ_i^{ex} from atomistic simulations, whereby a particle is randomly inserted into a given polymer configuration until the configurational average for $\exp(-\beta\Phi_t)$ is achieved. Independent polymer configurations are then sampled until the canonical ensemble average is obtained.

The test-particle insertion method has been used successfully at low to moderate fluid densities.[29] However, at high densities, the method becomes inefficient as it becomes increasingly unlikely that a test particle can be inserted successfully into the fluid. That is, it is much probable that a randomly chosen position in the high-density fluid will yield a large, positive value for Φ_t due to repulsive overlaps between the test particle and the host particles of the system. From eq 11 it is seen that these insertions will contribute negligibly to μ^{ex} because the Boltzmann factor for a large positive Φ_t makes a negligibly small contribution to the ensemble average. Significant improvements in insertion efficiencies can be achieved by searching only those regions of the fluid where successful particle insertions are more likely to occur, i.e., regions where negative or slightly positive values of Φ_t are obtained. Excluded-volume map sampling[25] (EVMS) is such a method for efficiently locating regions of high insertion probabilities.

C. Excluded-Volume Map Sampling. Within the framework of EVMS, the ensemble average in eq 11 is defined in terms of a normalized distribution function for Φ_t, $f(\Phi_t)$, as follows:[27]

$$\beta\mu^{ex}(\rho,T) = -\ln\int_{-\infty}^{\infty} d\Phi_t\, f(\Phi_t)\exp(-\beta\Phi_t) \qquad (12)$$

For large, positive values of Φ_t, the Boltzmann factor in eq 12 dominates and the contribution to the integral is essentially zero. Therefore, the integral may be cut off at a value $\Phi_t = \Phi_t^*$, defined such that negligible error in the integration is incurred. Equation 12 may then be rewritten as

$$\beta\mu^{ex}(\rho,T) = -\ln\int_{-\infty}^{\Phi_t^*} d\Phi_t\, f(\Phi_t)\exp(-\beta\Phi_t) \qquad (13)$$

Equation 13 is implemented in a simulation by sampling only those regions of the fluid in which the test particle may be inserted without repulsive overlaps with the host atoms. This implementation does not explicitly define Φ_t^*, but rather it simply excludes sites where substantial overlaps of the core repulsion would lead to high energies of insertion. Deitrick *et al.*[25] successfully applied this sampling method to calculate free energies for a pure LJ fluid at reduced densities greater than $\rho^* = 0.9$ ($\rho^* = \rho\sigma$). Sok *et al.*[4] also used the method to calculate excess chemical potentials of helium and methane in poly(dimethylsiloxane) (PDMS), and Tamai *et al.*[10] extended the approach to test particles with internal degrees of freedom.

Table 1. Summary of the Polystyrene Structures Studied in This Work

no. of monomers	box length (Å)	no. of structures	no. of monomers	box length (Å)	no. of structures
40	18.87	4	171	30.63	3
62	21.84	4	364	39.39	2

A modification to the EVMS method is used in this work. Rather than first calculating the distribution function $f(\Phi_t)$, $\langle \exp(-\beta\Phi_t)\rangle_N$ is directly evaluated as follows:

$$\langle \exp(-\beta\Phi_t)\rangle_N = \sum_{j=1}^{N_e}\frac{1}{N_{T_j}}\sum_{i=1}^{N_{V_j}}\exp(-\beta\Phi_{t_i}) \qquad (14)$$

where N_{V_j} is the number of sites in configuration j for which $\Phi_t < \Phi_t^*$, N_{T_j} is the total number of insertions for a given configuration j assuming a uniform insertion density, and N_e is the total number of configurations available for computing the ensemble average. While this approach is slightly more costly computationally, it reduces the error in μ^{ex} that arises from numerically evaluating $f(\Phi_t)$. This minor computational expense is not significant in comparison to the high computational costs of generating the polymer glass structures.

Candidate sites for insertion are defined as those for which the diameter of a hard-sphere probe does not overlap with the LJ diameter of any host atom. A simple and robust method for finding these sites is to place a $N \times N \times N$ lattice in the simulation box and determine whether the LJ radii of any host atoms fall within a fixed radius around each lattice node. If no host atoms are found within this search radius, the node is identified as unoccupied; if an overlap is encountered, the node is identified as occupied. Once all the unoccupied lattice nodes are located, test particles are inserted only at those nodes and their energy of interaction with the host atoms are calculated. Normalization of this biased sampling requires that the average for μ^{ex} for each configuration be weighted by $\omega_j = N_{V_j}/N_{T_j}$ before being summed to yield the desired ensemble average. Note that this procedure is very efficient if several different penetrants are to be examined, as is the case here, since the excluded-volume map needs to be generated only once for each structure.

III. Computational Methodology

A. Glass Generation. For different sizes of atactic polystyrene glass have been generated, spanning nearly an order of magnitude in molecular weight. The size and number of each structure is listed in Table 1. All structures consist of a single parent chain confined to a periodic cube at a density of 1.03 g/cm^3 with the average fraction of mesodiads equal to 0.5.[24]

Initial starting configurations for the 40-mers were generated using a simulated polymerization technique.[15] The three larger sizes were generated using a new Gaussian lattice algorithm, which can efficiently generate much longer chains with a specified tacticity. Details of the method are described elsewhere;[24] however, we note here an important consequence of this algorithm is that it ensures the chain is Gaussian on all length scales. Each structure was subjected to the same annealing schedule to remove any structural artifacts resulting from the generation methods. This schedule entailed energy minimization of the initial

structures to mechanical equilibrium at 0 K to remove high-energy overlaps and distorted bond lengths and angles. Molecular dynamics (MD) was then performed at 1000 K for 300 ps, followed by the production run at 300 K for 200 ps. The last 100 ps from the 300 K MD simulations were used for structural analysis as well as for calculating gas solubilities.

Note that since a chain with the proper Gaussian statistics on all length scales is obtained, polymer annealing is used only to relax the local chain environment. These local relaxations include relaxation of distorted bond angles and bond lengths as well as nonbonded van der Waals interactions. In performing the annealing, any vestiges of the initial lattice chain are removed.[24] Thus, while the Gaussian lattice generation method assures *a priori* that the chain topology is correct on all length scales, annealing ensures the local environment is relaxed. The annealing schedule was determined by following the change in the X-ray structure factor as a function of time. Initial structure factor calculations showed sharp/distinct peaks resulting from the lattice generation method; however, these features were removed during annealing to give final structure factors that agree well with experimental patterns.

The MD simulations at 1000 K were executed using a time step of 1.0 fs with SHAKE applied to all bonds and a 4.0 Å potential cutoff distance to increase computational efficiency. The MD simulations at 300 K were executed using a time step of 2.0 fs with SHAKE applied only to C−H bonds and a 9.0 Å potential cutoff distance. All energy minimizations and MD calculations were performed using AMBER 4.1 and its associated force-field expressions and parameters for bond stretching, bond angle bending, torsion angle rotation, and van der Waals nonbonded interactions.[30] Electrostatics interactions in the AMBER force-field expression are treated using a distance-independent dielectric constant and partial charges determined by a Mulliken population analysis of AM1 semiempirical molecular orbital calculations on polystyrene dimers and trimers.[15]

B. Selection of EVMS Parameters. The lattice spacing and search radius for the modified EVMS (M-EVMS) algorithm were chosen by balancing computational efficiency and precision. A search radius too small and a lattice spacing too fine lead to excessively high computational demands, while not significantly increasing the precision of the algorithm. A search radius too large and a lattice spacing too coarse exclude regions that contribute to the excess chemical potential, resulting in its overprediction.

The optimum choices for lattice spacing and search radius were identified as follows. A cubic lattice with 0.1 Å between nodes was placed in a single 62-mer configuration. An argon atom, the smallest particle considered in this work, was inserted at each node, and the excess chemical potential was calculated using eq 14. This value is taken to be the "true" value for Ar in this configuration. A series of search radii from 0.5 to 1.5 Å and lattice spacings from 0.1 to 0.5 Å were then used to calculate excess chemical potentials with the M-EVMS algorithm. The parameters reproducing the true excess chemical potential of Ar to within 0.01% in the least computational time were then selected. Note that the sampling time scales roughly with the inverse cube of the lattice spacing and increases with decreasing search radius. The excess chemical potentials calculated using different combinations of search radii and lattice spacings are reported in Table 2. For this work, the optimum parameters were found to be 0.3 Å for the lattice spacing and 1.0 Å for the search radius.

Table 2. Values of the Excess Chemical Potential for Ar in a 62-mer Polystyrene Glass Calculated Using the M-EVMS Algorithm with the Given Search Radius and Lattice Spacing

search radius (Å)	lattice spacing (Å)				
	0.1	0.2	0.3	0.4	0.5
0.50	0.515	0.515	0.515	0.516	0.505
0.75	0.515	0.515	0.515	0.516	0.505
1.00	0.515	0.515	0.515	0.516	0.505
1.25	0.589	0.589	0.594	0.586	0.573
1.50	1.231	1.215	1.256	1.364	1.421

Table 3. Lennard-Jones Potential Parameters for Gases[18]

gas	ϵ (kcal/mol)	σ (Å)	gas	ϵ (kcal/mol)	σ (Å)
N_2	0.1888	3.698	CH_4	0.2943	3.817
O_2	0.2333	3.580	CO_2	0.3753	4.486
Ar	0.2379	3.405			

Table 4. Comparisons of Sampling Times for the M-EVMS Algorithm and Random Insertion

no. of atoms in system	no. of insertions	M-EVMS time (s)	random sampling time (s)
642	250 047	19	705
994	389 017	33	1503
2738	1 092 727	152	3071
5826	2 248 091	376	11568

C. Calculation of the Excess Chemical Potentials by M-EVMS. Infinite-dilution excess chemical potentials were calculated for five gases: N_2, O_2, Ar, CH_4, and CO_2, represented as LJ spheres. We note that the choice of modeling these penetrants as LJ spheres is motivated by experimental solubility data, which shows a linear correlation of the logarithm of the Henry's law constant with LJ well depth.[23] Since we are interested in probing the polymer glasses for system size effects rather than optimizing potentials to quantitatively reproduce experimental data, we use LJ parameters extracted from second virial coefficients (Table 3). LJ interactions between these gases and the polymer atoms are defined by applying the standard Lorentz−Berthelot mixing rules. The potential is truncated at 9 Å, and standard corrections are made for longer-range interactions.[31] Excess chemical potentials were calculated every 5 ps over the last 100 ps of the 300 K MD trajectories. This rate of sampling was chosen based on a calculation of the statistical inefficiency,[31] which determines the number of time steps that must be skipped before the next configuration in the time series may be considered an independent contribution to the ensemble average.

As expected, a significant increase in efficiency with equivalent or better accuracy was obtained by applying the M-EVMS algorithm compared to random sampling. Table 4 documents the efficiency of M-EVMS versus random sampling for an equivalent number of test-particle insertions. In general, the M-EVMS algorithm is between 10 and 40 times faster than random sampling, a consequence of the fact that the EVMS algorithm identifies only $\sim^1/_{10} - {}^1/_{40}$ of the total number of sites as contributing insertion sites. We note that the algorithm also scales linearly with system size, indicating that it will remain efficient when used in conjunction with systems even larger than those studied here.

IV. Results and Discussion

The results for the calculated excess chemical potential as a function of the LJ well-depth parameter, ϵ, of

Table 5. Summary of Calculated the Excess Chemical Potentials (kcal/mol) in Atactic Polystyrene Glasses at 300 K and 1.03 g/cm^3 [a]

	N_2	O_2	Ar	CH_4	CO_2
40-mer	1.05 ± 0.76	0.56 ± 0.65	0.44 ± 0.48	0.32 ± 1.08	3.47 ± 4.47
62-mer	0.78 ± 0.41	0.34 ± 0.34	0.28 ± 0.24	−0.11 ± 0.58	1.27 ± 2.53
171-mer	0.75 ± 0.59	0.35 ± 0.54	0.32 ± 0.46	−0.17 ± 0.73	−0.28 ± 2.51
364-mer	0.61 ± 0.12	0.23 ± 0.10	0.22 ± 0.07	−0.38 ± 0.16	−1.42 ± 0.63

[a] The standard deviations are based on 5 ps block averages over the 100 ps sampling.

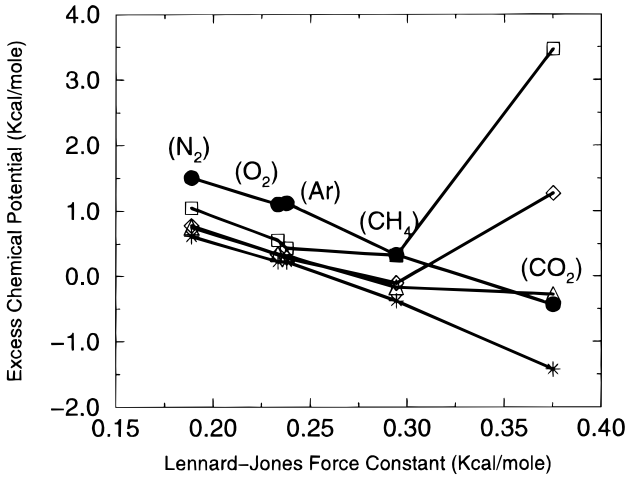

Figure 1. Calculated excess chemical potentials at 300 K and a polymer density of 1.03 g/cm^3 for the LJ gases as a function the LJ well depth of the sorbed gas (error bars are not shown for clarity but are given in Table 5): (●) experimental data,[23,32] (□) 40-mer, (◇) 62-mer, (△) 171-mer, (∗) 364-mer.

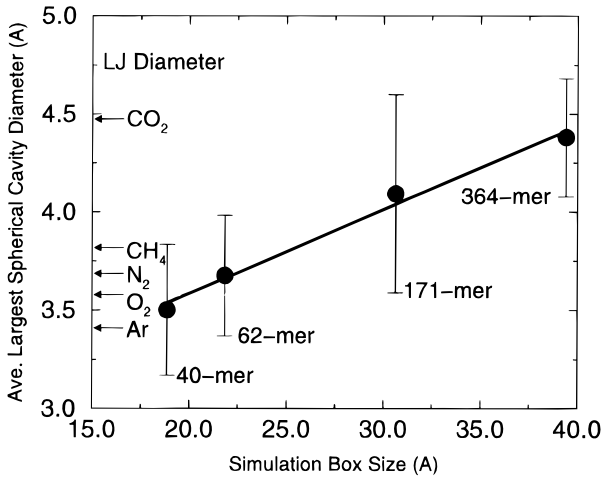

Figure 2. Average largest spherical cavity (LSC) found in each size polystyrene structure. LJ diameters for the penetrant gases are indicated on the *y*-axis for reference. The average is calculated from configurations taken every 5 ps over the 100 ps MD production run.

the sorbed gas are shown in Figure 1 for the different system sizes. For comparison, experimental excess chemical potentials derived from reported gas solubilities at 300 K and 1 atm in unoriented atactic polystyrene glass are included.[23,32] The calculated excess chemical potentials with estimates of their standard deviations are also given in Table 5.

A linear correlation is observed for the largest system size (364-mer), with the calculated excess chemical potentials uniformly shifted down from the experimental values by approximately 1 kcal/mol (Figure 1). This qualitative behavior is in excellent agreement with experiment, especially since no optimization of the forcefield parameters was attempted. Overestimations of gas solubilities of similar magnitude have been reported in the literature[4,7] and are commonly ascribed to inaccuracies of the potential functions.[4,10] Tuning the potential parameters by either modification of the LJ ϵ or σ parameters and/or modification of the Lorentz−Berthelot mixing rules is expected to lead to quantitative agreement, as found in other work.[7] We note that, while quantitative agreement between our simulations and experiment is not achieved, the results for the 364-mer allow for the quantitative prediction of relative gas solubilities in polystyrene glass and, more importantly, for a systematic examination of system size effects.

The most striking feature of the results displayed in Figure 1, however, is the large deviation from the linear correlation for CO_2, and to some degree CH_4, evident in the smaller structures. The excess chemical potentials for N_2, O_2, and Ar are not statistically different from one another among the different ensemble sizes. In contrast, CO_2 has a significantly higher excess chemical potential in the smaller structures, indicating that interactions between CO_2 and the polymer matrix are less favorable in these structures. These less favorable interactions result from a larger number of high-energy (overlapping) configurations when CO_2 is inserted into the polymer matrix, which we hypothesize is a consequence of an absence of cavities within the matrix that are of sufficient size to accommodate the larger gas molecule in the smaller structures.

To test for the presence of large cavities in the different sized structures, we have determined the largest spherical cavity (LSC) that can be found in each structure. The LSC for an individual configuration is found by placing a cubic lattice (0.1 Å between nodes) in the polymer and calculating the distance from each node to the nearest-neighbor polymer atom. Adjoining, unoccupied nodes define the LSC. We calculate the LSC in each structure for configurations sampled every 5 ps from the last 100 ps of the 300 K MD trajectories. An average value for each structure size is reported in Figure 2, plotted versus the simulation box size. Although there is significant scatter in the results, it is clear that the average value of the LSC increases with increasing box size. For comparison, the LJ diameters of the gases are shown along the *y*-axis. In the 40-mer, the LJ diameters of Ar, O_2, and N_2 are within $^1/_2$ of a standard deviation of the average LSC value, while CH_4 is at 1 standard deviation and CO_2 is approximately 3 standard deviations above the average value of the LSC. Since the dominant contributions to the excess chemical potential calculations arise from cavities large enough to accommodate the gases, the small probabilities of finding cavities sufficiently large for CO_2 and CH_4 lead to anomalously high values of μ^{ex}. Similarly, in the 62-mer, CO_2 is more than a standard deviation above the average LSC value and its excess chemical potential remains anomalously high relative to the other gases (Figure 1). It is not until the box size reaches 39.39 Å (364-mer) that the probability of finding a cavity to accommodate CO_2 is significant enough to yield a reasonable value for μ^{ex} as defined by the linear correlation in Figure 1. Thus, the absence of larger cavities in the smaller structures decreases the probability for

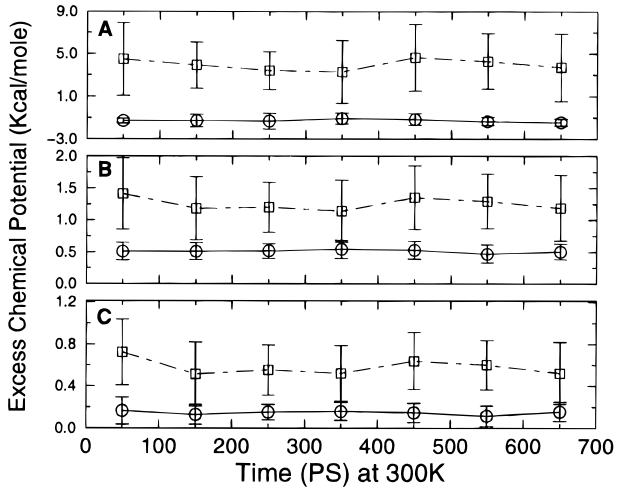

Figure 3. Excess chemical potential for 62-mer (- −□- −) and 171-mer (−○−) structures averaged in 100 ps intervals. Averages were calculated from two structures of each size. (A) CO_2, (B) N_2, (C) Ar.

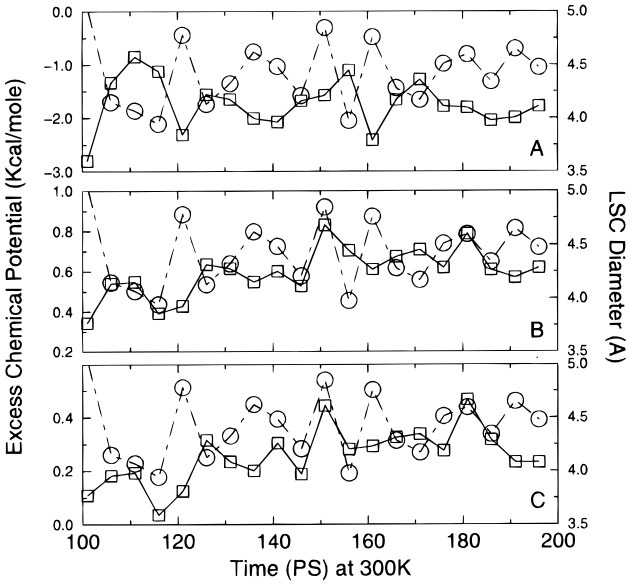

Figure 4. Correlation between the excess chemical potential (□) and the largest spherical cavity (○) within a 364-mer microstructure as a function of time: (A) CO_2, (B) N_2, (C) Ar.

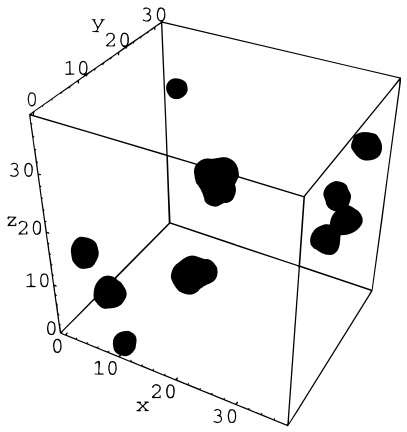

Figure 5. Positions in a single 364-mer configuration where the total energy of interaction for inserting CO_2 is favorable. The polymer has been removed for ease of visualization.

successful insertion of the larger gases. Figures 1 and 2 also indicate that the test-particle insertion technique fails for test particles larger than $^1/_2$ of a standard deviation above the average diameter of the LSC in the structure under consideration. We note that alternative methods such as thermodynamic integration,[33] although computationally costly, could be employed to force the formation of large cavities in these systems. The accuracy and efficiency of such techniques have not been investigated here.

We have tested structures produced by the Gaussian lattice generation method to ensure that the annealing time is not a function of simulation size. Once the local environment has been relaxed, the polymer is in a stable minimum-energy state. We do not expect the cavity distribution or the mean values of the excess chemical potential to change significantly with time. Figure 3 supports this conclusion. We have performed an additional 600 ps of MD on two 62-mer and two 171-mer structures and calculated the mean value of the excess chemical potential in 100 ps block intervals. These values are then averaged and plotted versus time in Figure 3, where it is seen that the excess chemical potential is essentially constant. Thus, the excess chemical potential calculated from the 100 ps trajectories is representative of the relaxed, glass structure.

During the 100 ps trajectories at 300 K from which μ^{ex} is calculated, large-scale relaxation of the polymer such as cooperative trans−gauche transitions along the chain backbone, as well as more localized relaxations such as benzene ring flips,[34] are not expected. Instead, the polymer will fluctuate around its local minimum-energy configuration. These fluctuations create small cavities (i.e., <2 Å diameter) and allow large cavities to "breathe" or fluctuate in size. Figure 4 shows the instantaneous values of μ^{ex} for CO_2, N_2, and Ar and the corresponding LSC for one of the 364-mer structures over the course of the 100 ps trajectory. (Note that the plots in Figure 4 have different scales for the excess chemical potential.) From Figure 4A, it is apparent that $\mu^{ex}_{CO_2}$ exhibits a strong inverse correlation with the LSC fluctuations. The reciprocal correlation coefficient is 0.84 for CO_2 but only 0.08 and 0.12 for N_2 (Figure 4B) and Ar (Figure 4C), respectively.

One explanation for the much stronger correlation of $\mu^{ex}_{CO_2}$ with the LSC is that there is a single cavity within the structure that is able to accommodate CO_2 (that is, the LSC) and this cavity alone determines the value of the excess chemical potential. Small fluctuations in the size or shape of this cavity would greatly affect the insertion probability for CO_2 and thus μ^{ex}. Such large, single cavities within atomistic polymer glass structures have been reported in polyisobutylene[7] and were found to represent the bulk of the contributions to the calculated excess chemical potential for O_2 in these structures. However, upon examination of our structures, no single large cavity is evident. Figure 5 shows those positions in a representative 364-mer configuration where the total potential energy of interaction for inserting CO_2 is favorable (the polymer has been removed for clarity of vizualization). On the order of seven distinct cavities are identified into which CO_2 can be successfully inserted, with three cavities contributing 95% of the excess chemical potential. The high correlation between the excess chemical potential of CO_2 and the LSC is attributed to the fact that the diameter of the LSC (4.4 ± 0.35 Å) is comparable to the LJ diameter of the CO_2 (4.486 Å) molecule itself. Therefore, fluctuations in the LSC, whichever of the three dominant cavities it is, will be strongly correlated with $\mu^{ex}_{CO_2}$. In contrast, for small molecules such as N_2 and Ar with LJ diameters of 3.698 and 3.405 Å, respectively, there are on the order of 12 (N_2) and 17 (Ar) cavities which

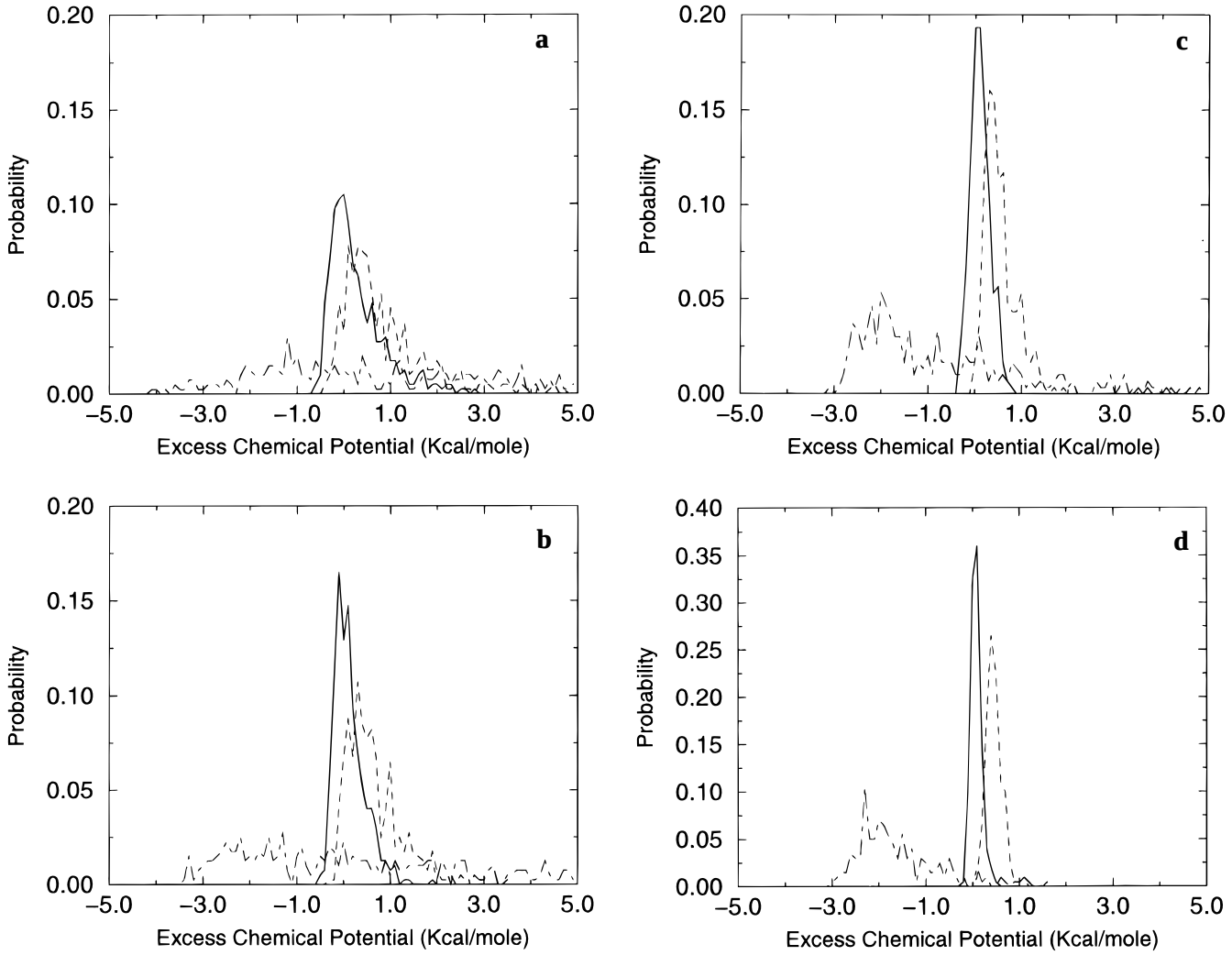

Figure 6. Distributions of the excess chemical potential for Ar (—), N_2 (– –), and CO_2 (– - –) in the four different sized polystyrene structures: (a) 40-mer, (b) 62-mer, (c) 171-mer, (d) 364-mer.

contribute 95% of the excess chemical potential. Because these gases are significantly smaller than the LSC and there are many more accessible cavities that are smaller in size, the excess chemical potentials of both N_2 and Ar are not sensitive to the fluctuations of any single cavity or to fluctuations in the size of the largest cavity.

Parts a−d of Figure 6 show the distributions of instantaneous values of the excess chemical potentials for Ar, N_2, and CO_2 in the four different sized structures obtained by sampling configurations once every 5 ps from the last 100 ps of the MD trajectories. For the ensembles to be free of system size effects, the distribution of μ^{ex} should be peaked around a well-defined maximum that does not change with system size. Upon examination of Figure 6a−d (note the change in scale of the *y*-axis in Figure 6d), it is apparent that the peak in the distribution of μ^{ex} for all three gases becomes more pronounced with increasing simulation size. For both Ar and N_2, the mean value does not change significantly with increasing size. This is in contrast to the distributions of μ^{ex} for CO_2. In the 364-mer (Figure 6d), this distribution has an identifiable, although not well-defined, maximum. As the simulation size decreases, this visible maximum vanishes. Additionally, the mean value of μ^{ex} changes considerably, as is also evident in Figure 1 and Table 5. The lack of a well-defined, single peak in the distribution signals the lack of cavities. Thus, the distribution of μ^{ex} provides a more sensitive test of system size effects than the use of only the mean value of μ^{ex}.

No single cause has been identified as being responsible for the suppression of large cavities in the smaller structures. It has been noted recently[24] that simulations of polystyrene in box sizes less than 25−30 Å introduce a deterministic, systematic error in the residue-based calculation of the electrostatic interactions. That is, if a residue is located at the potential cutoff, the entire residue must be included in the electrostatic calculation to maintain electroneutrality. However, if the residue and the potential cutoff sum to more than half the box length, the periodic boundary conditions will split the residue, creating an artificial dipole. Undoubtedly, these artificial dipoles will affect the polymer structure and hence the cavity distributions. We note that, for polystyrene, the sum of the residue length and potential cutoff distance is slightly more than 14 Å; thus, the two smaller structures used in this work and in other studies using residue-based cutoffs may be subjected to this error.

V. Conclusions

Strong system size effects have been found in our simulations of simple gases sorbed in amorphous polystyrene glass. Specifically, the diameter of the largest spherical cavity in the polymer structure increases from approximately 3.5 to 4.5 Å as the simulation box length is doubled from approximately 20 to 40 Å (Figure 2).

Moreover, the distribution of instantaneous μ^{ex} values of the sorbed gases becomes more pronounced (Figure 6) as the simulation box length increases over this range. These results suggest that the higher solubilities observed for larger gas molecules (e.g., CH_4 and CO_2) in the larger polymer structures are due to the presence of cavities of sufficient size to accommodate these molecules.

Our results also show that the simulation size required for the calculation of μ^{ex} increases with increasing van der Waals radius of the penetrant. For CO_2 in atactic polystyrene, a 364-mer is required to yield a reasonable value of the excess chemical potential as defined by the linear correlation of the experimental data in Figure 1. In contrast, the smaller structures yield artificially low probabilities for successful CO_2 insertion and, consequently, anomalously high values for the excess chemical potential. For the sorption of smaller molecules, such as Ar or N_2, polymer structures as small as the 62-mers yield reasonable μ^{ex} values. Further, the distribution of μ^{ex} values provides a measure of the compatibility of a generated glass structure of a particular size for a penetrant of interest. Finally, we note that our implementation of a modified EVMS algorithm is a robust and efficient method for calculating the excess chemical potential of small penetrants in large atomistic simulations of amorphous polymer glasses.

Acknowledgment. We gratefully acknowledge the financial support provided by the Dow Chemical Company, the National Science Foundation Fellowship DGE-9253850, and a Delaware Research Partnership. We further thank the Cornell Theory Center, which receives major funding from the National Science Foundation and New York State, the Advanced Research Projects Agency, the National Institutes of Health, IBM Corporation, and members of the center's Corporate Research Institute, for the use of their facilities and equipment.

References and Notes

(1) Gusev, A. A.; Suter, U. W. Theory for solubility in static systems. *Phys. Rev. A* **1991**, *43*, 6488−6494.
(2) Mueller-Plathe, F. Calculation of the free energy for gas absorption in amorphous polypropylene. *Macromolecules* **1991**, *24*, 6475.
(3) Mueller-Plathe, F.; Rogers, S. C.; van Gunsteren, W. F. Diffusion coefficients of penetrant gases in polyisobutylene can be calculated correctly by molecular dynamics simulations. *Macromolecules* **1992**, *25*, 6722−6724.
(4) Sok, R. M.; Berendsen, H. J. C.; van Gunsteren, W. F. Molecular dynamics simulation of the transport of small molecules across a polymer membrane. *J. Chem. Phys.* **1992**, *96*, 4699.
(5) Gusev, A. A.; Suter, U. W. Dynamics of small molecules in dense polymers subject to thermal motion. *J. Chem. Phys.* **1993**, *99*, 2228.
(6) Pant, P. V.; Boyd, R. H. Molecular dynamics simulation of diffusion of small penetrants in polymers. *Macromolecules* **1993**, *26*, 679−686.
(7) Mueller-Plathe, F.; Rogers, S. C.; van Gunsteren, W. F. Gas sorption and transport in polyisobutylene. *J. Chem. Phys.* **1993**, *98*, 9895.
(8) Gusev, A. A.; Mueller-Plathe, F.; van Gunsteren, W. F.; Suter, U. W. Dynamics of small molecules in bulk polymers. *Adv. Polym. Sci.* **1994**, *116*, 209−246.
(9) Tamai, Y.; Tanaka, H.; Nakanishi, K. Molecular simulation of permeation of small penetrants throught membranes. 1. Diffusion coefficients. *Macromolecules* **1994**, *27*, 4498−4508.
(10) Tamai, Y.; Tanaka, H.; Nakanishi, K. Molecular simulation of permeation of small penetrants through membranes. 2. Solubilities. *Macromolecules* **1995**, *28*, 2544−2554.
(11) Gusev, A. A.; Suter, U. W.; Moll, D. J. Relationship between helium transport and molecular motions in a glassy polycarbonate. *Macromolecules* **1995**, *28*, 2582−2584.
(12) Theodorou, D. N.; Wuter, U. W. Detailed molecular structure of a vinyl polymer glass. *Macromolecules* **1985**, *18*, 1467−1478.
(13) McKechnie, J. I.; Brown, D.; Clarke, J. H. R. Methods of generating dense relaxed amorphous polymer samples for use in dynamic simulations. *Macromolecules* **1992**, *25*, 1562−1567.
(14) Boyd, R. H.; Pant, P. V. Simulation of glassy polymethylene starting from the equilibrated liquid. *Macromolecules* **1991**, *24*, 4078−4083.
(15) Khare, R.; Paulaitis, M. E.; Lustig, S. R. Generation of glass structures for molecular simulation of polymers containing large monomer units; application to polystyrene. *Macromolecules* **1993**, *26*, 7203−7209.
(16) Roe, R. J. Short time dynamics of polymer liquid and glass studied by molecular dynamics simulation. *J. Chem. Phys.* **1994**, *100*, 1610−1619.
(17) Hutnik, M.; Gentile, F. T.; Ludovice, P. J.; Suter, U. W.; Argon, A. S. An atomistic model of the amorphous glassy polycarbonate of 4,4′-isopropylidenediphenol. *Macromolecules* **1991**, *24*, 5962−5969.
(18) Hirschfelder, J. O.; Curtiss, C. F.; Bird, R. B. *Molecular Theory of Gases and Liquids*; John Wiley and Sons, Inc.: New York, 1954.
(19) Valleau, J. P. *Modern Theoretical Chemistry: V5, Chapter 5—A guide to Monte Carlo for statistical mechanics*; Plenum Press: New York, 1977.
(20) Takeuchi, H. A jump motion of small molecules in glassy polymers: A molecular dynamics simulation. *J. Chem. Phys.* **1990**, *93*, 2062−2067.
(21) Mueller-Plathe, F.; Laaksonen, L.; van Gunsteren, W. F. Cooperative effects in the transport of small molecules through an amorphous polymer matrix. *J. Mol. Graphics* **1993**, *11*, 118−120.
(22) Reiss, H. Scaled particle methods in the statistical thermodynamics of fluids. *Adv. Chem. Phys.* **1965**, *9*, 1−84.
(23) Veith, W. R.; Tam, P. M.; Michael, A. S. Dual sorption mechanisms in glassy polystyrene. *J. Colloid Interface Sci.* **1966**, *22*, 360−370.
(24) Kotelyanskii, M. J.; Wagner, N. J.; Paulaitis, M. E. Building large amorphous polymer structures: Atomistic simulation of glassy polystyrene. *Macromolecules* **1996**, *29*, 8497−8506.
(25) Deitrick, G. L.; Scriven, L. E.; Davis, H. T. Efficient molecular simulation of chemical potentials. *J. Chem. Phys.* **1989**, *90*, 2370−2385.
(26) Prausnitz, J. M.; Lichtenthaler, R. N.; de Azevedo, E. G. *Molecular Thermodynamics of Fluid-Phase Equilibria*, 2nd ed.; Prentice-Hall Inc.: Englewood Cliffs, NJ, 1986.
(27) Shing, K. S.; Gubbins, K. E. The chemical potential in dense fluids and fluid mixtures via computer simulation. *Mol. Phys.* **1982**, *46*, 1109−1128.
(28) Widom, B. Some topics in theory of fluids. *J. Chem. Phys.* **1963**, *39*, 2808−2811.
(29) Torrie, G. M.; Valleau, J. P. Monte Carlo free energy estimates using non-Boltzmann sampling. *Chem. Phys. Lett.* **1974**, *28*, 578−581.
(30) Weiner, S. J.; Kollman, P. A.; Case, D. A.; Singh, U. C.; Ghio, C.; Alagona, G.; Profeta, S.; Weiner, P. A new force-field for molecular mechanical simulation of nucleic acids and proteins. *J. Am. Chem. Soc.* **1984**, *106*, 765−784.
(31) Allen, M. P.; Tildesley, D. J. *Computer Simulation of Liquids*; Clarendon Press: Oxford, U.K., 1993.
(32) Kuzina, S. I.; Mikhailov, ,A. I. The solubility of gases in polymers at low temperatures. *Polym. Sci. USSR* **1992**, *34*, 130−134.
(33) Beutler, T. C.; Beguelin, D. R.; van Gunsteren, W. F. Free energy of cavity formation in solvent: Computational methodological, and physical aspects. *J. Chem. Phys.* **1995**, *102*, 3787.
(34) Khare, R.; Paulaitis, M. E. Molecular simulations of cooperative ring flip motions in bulk polystyrene glass. *Macromolecules* **1995**, *28*, 4495−4504.

MA960776D